Available online at www.sciencedirect.com

jmr&t Journal of Materials Research and Technology

journal homepage: www.elsevier.com/locate/jmrt

Original Article

Revealing twinning from triple lines in nanocrystalline copper via molecular dynamics simulation and experimental observation

Silu Liu [a], Jian Yin [b], Yonghao Zhao [a,*]

[a] Nano and Heterogeneous Materials Center, School of Materials Science and Engineering, Nanjing University of Science and Technology, Nanjing, 210094, PR China

[b] Power Plant Life Management Research Center, Suzhou Nuclear Power Research Institute, Suzhou, 215004, PR China

ARTICLE INFO

Article history:
Received 20 October 2020
Accepted 9 January 2021
Available online 16 January 2021

Keywords:
Nanocrystalline Cu
MD
TKD
Triple line/junction
Twinning

ABSTRACT

As the intersecting line of three grain boundaries (GBs), triple line is in non-equilibrium state with large stress concentration and extra energy, which makes it the optimal site for twin nucleation. However, it is very difficult to verify this conjecture by direct experiments, so no one has done it so far. In present work, we try to use molecular dynamics (MD) simulation on nanocrystalline Cu to confirm such hypothesis. We found that 25 out of 28 twins were emitted from triple lines. The related atomic micro-mechanism has been analysed. Stress relaxation and energy reduction were considered to be the driving factors for twinning from triple lines. This could be proved by changes of dihedral angles, relative GB energy sum, average atomic von Mises shear stress and average atomic energy. Experimentally, the transmission Kikuchi diffraction (TKD) characterization on nanocrystalline Cu revealed that the fraction of the triple junction-twin intersection was 81.7% in all twinned nanograins. The underestimation of experimental results might be caused by invisible triple lines in the orientation mapping.

1. Introduction

In the past two decades, in addition to the grain boundary (GB) related deformation mechanism, twinning has also been revealed as one of the main deformation mechanisms for nanocrystalline (nc) face-centered-cubic (fcc) metals and alloys with low to medium stacking fault energy [1]. Twinning mechanism in nc fcc metals and alloys via partial dislocation emission from GBs was firstly predicted by molecular dynamics (MD) simulation and then firmly verified by high resolution transmission electron microscopy (HRTEM) [1–5]. A large number of subsequent studies show that twinning can also improve the ductility of nc metals and alloys [1]. Up to now, it has been widely accepted that partial dislocations could readily be emitted from non-equilibrium GBs to nucleate a deformation twin [6–9].

* Corresponding author.
E-mail address: yhzhao@njust.edu.cn (Y. Zhao).

https://doi.org/10.1016/j.jmrt.2021.01.033

A triple line is the intersection of three GBs of three adjacent grains, which is also called triple junctions when it's perpendicular or edge-on to the observation plane [10,32]. As the intersection of three GBs, triple lines are considered to be in a severely unbalanced state due to lattice mismatch. Or to put it another way, as the consequence of lattice mismatch and surplus defects, large strain and stress concentrate in triple lines, imposing them high line tension or energy [8–12]. Therefore, triple lines has been revealed as sinks and emitters of free volumes, dislocations and other defects, [3,8,9]. Since the total excess free energy of triple lines is enhanced, they are easier to overcome the energy barrier to participate into the GB-related deformation mechanisms. It has also been demonstrated that triple lines are energetically more favorable than GBs. They would play increasingly important role as the grain size gets smaller [11–14].

With high energy non-equilibrium state, triple junctions or lines have been reported to play a critical role in GB-mediated deformation mechanisms of nc materials, such as the grain rotation [15], GB sliding [16] and nucleation of nanovoids [17]. Growth twins have also been observed to nucleate at triple lines in Ni during annealing [13]. Our earlier work [18] also discovered that 83% of all characterized nc Cu–Zn grains have at least one twin being intersected with a triple line. Nevertheless, the distinction between GB and triple line has been unable to arouse sufficient attention from researchers in terms of stress and energy. Instead, they were usually bound together and called interface stress and energy [12]. Such practice might mask the important role played by the local stress and energy associated with the triple line in a variety of issues [12,19]. Therefore, we hypothesized that the triple line was more effective in promoting partial dislocation emissions and nucleating twins than GBs during the deformation of nc fcc metals and alloys.

The hypothesis above remains poorly researched because vast percentages of twinning from triple lines are opaque to visible light and electron beams [13]. Firstly, only triple lines normal in view could be characterized as triple junctions by standard probes, but those triple lines would stay invisible when being parallel in view. Furthermore, twinning nucleated from triple lines is an evolving process with strain in three-dimensional space and therefore could hardly be captured by light or electron beam probes as a panoramic view. On the basis of above problems, in this work we employed MD simulation to directly visualize twin nucleation and growth process in nc Cu under shear stress. In addition, we further employed the transmission Kikuchi diffraction (TKD) characterization to reveal the fraction of the triple junction-twin intersections in all twinned Cu nanograins.

2. Experimental methods

2.1. MD simulation

Herein, MD simulation was carried out by using the Large-scale Atomic/Molecular Massively Parallel Simulator (LAMMPS) code [20]. This work applied the embedded atom method (EAM) interatomic potential of Cu [21] to describe the interaction between atoms. The atomic configuration could be visualized by making use of the Ovito software [22].

The simulation model had a dimension of 40 nm × 40 nm × 40 nm with 6 grains and an average grain size of about 22.01 nm 5,418,858 Cu atoms in the simulation box were coded by colors based on common neighbor analysis (CNA) calculation [23,24]. Green, red, blue and white dots represented fcc, hexagonal close packed (hcp), body centered cubic (bcc) and GB atoms, respectively. The initial nc structure was constructed by the Voronoi tessellation method with Atomsk software [25]. Each grain in the model had random center point and crystallographic orientation. Periodic boundary conditions were then applied along all three directions. The simulation was performed in isothermal-isobaric NPT ensemble at room temperature (300 K) while pressure along Z direction was controlled being around 0 GPa. In the simulation, the initial model was firstly energy minimized by conjugate gradient (CG) algorithm and then relaxed for about 10 ps to obtain equilibrium structure at 300 K. A X–Y shear deformation was applied to the simulation box at a constant strain rate (10^9 s^{-1}). The simulation process ran about 150 ps and the total shear strain was 0.15.

2.2. Material and TKD characterization

The commercial Cu sheet with the thickness of 1 mm was first annealed at 973 K for 3 h to achieve homogeneous microstructure and then punched into ϕ10 mm disks for high pressure torsion (HPT) processing. We conducted the HPT processing at room temperature for 10 revolutions with an imposed pressure of 1 GPa at a speed of 1.5 rpm. To get electron-transparent TKD foils, the as-deformed disks were mechanically grinded and subsequently electropolished by double-jet electropolishing. The TKD foils were punched from the disk peripheries which had the greatest degree of grain refinement. The electrolyte for electropolishing was $1H_3PO_4$: $1C_2H_5OH$: $2H_2O$. This research carried out the TKD characterization in a Zeiss Auriga scanning electron microscope under the accelerating voltage of 30 kV. The measurement step size was set to 6 nm. The noise reduction for collected datasets could remove mis-indexed points and filter out some non-indexed pixels.

3. Results and discussion

3.1. Twinning from triple lines

Fig. 1 illustrates snapshots on typical sequences of twin nucleating and emitted from triple line in the MD simulation. For better vision, green fcc atoms were removed from our MD simulation results. As shown in Fig. 1(a), there were two triple lines (TL1 and TL2) and they were bounded by grains of G1, G2, G3 and grains of G2, G3, G4, respectively. G23 was the GB between grains G2 and G3. When the shear strain reached 3%, there were many local areas of red atoms with short range order in G23, some of them (F1 and F2) were originated from TL1 while some others (F3 and F4) from TL2. Fig. 1(b) demonstrates that red local areas with short range order grew and became enlarged when the shear strain increased

to 4%. These local areas (F1–F5) with short range order were structure or phase fluctuations. Under proper condition, these fluctuations could develop into twin nuclei as twin embryos. Twin embryos below the critical size are still unstable and will likely disappear. Herein, a lot of red twin embryos were just energy fluctuations. To grow into a stable twin embryo and emit a twin, it was indispensable for the partial dislocation to slip on proper slip system under loading to meet the requirement of stress and overcome the energy barrier [26]. Additionally, the total energy after twinning should be reduced to make the system more stable. Undoubtedly, stress concentration could also be relaxed during twinning [27].

In Fig. 1(c-e), when the shear strain was 6%, a stable deformation micro-twin (F1) was emitted into the grain G2 by the partial dislocation emissions from the twin nucleus in TL1. In a perfect fcc lattice, the close-packed planes {111} are stacked in the sequence ABCABCABC … as green fcc interior atoms in Fig. 1(f). In Fig. 1(f), the micro-twin (F1) was generated by the emission of three stacking faults SF1-SF3. According to atom sites in the three-dimensional space of MD simulation, the first stacking fault SF1 in Fig. 1(f) was emitted as the initial layer A atoms slipped in the <112> direction to a B layer position (i.e. the first row of red atoms on the left in Fig. 1(f)). In the same way, the next initial layer B atoms slipped to a C layer position (i.e. the row of green atoms in the middle of two

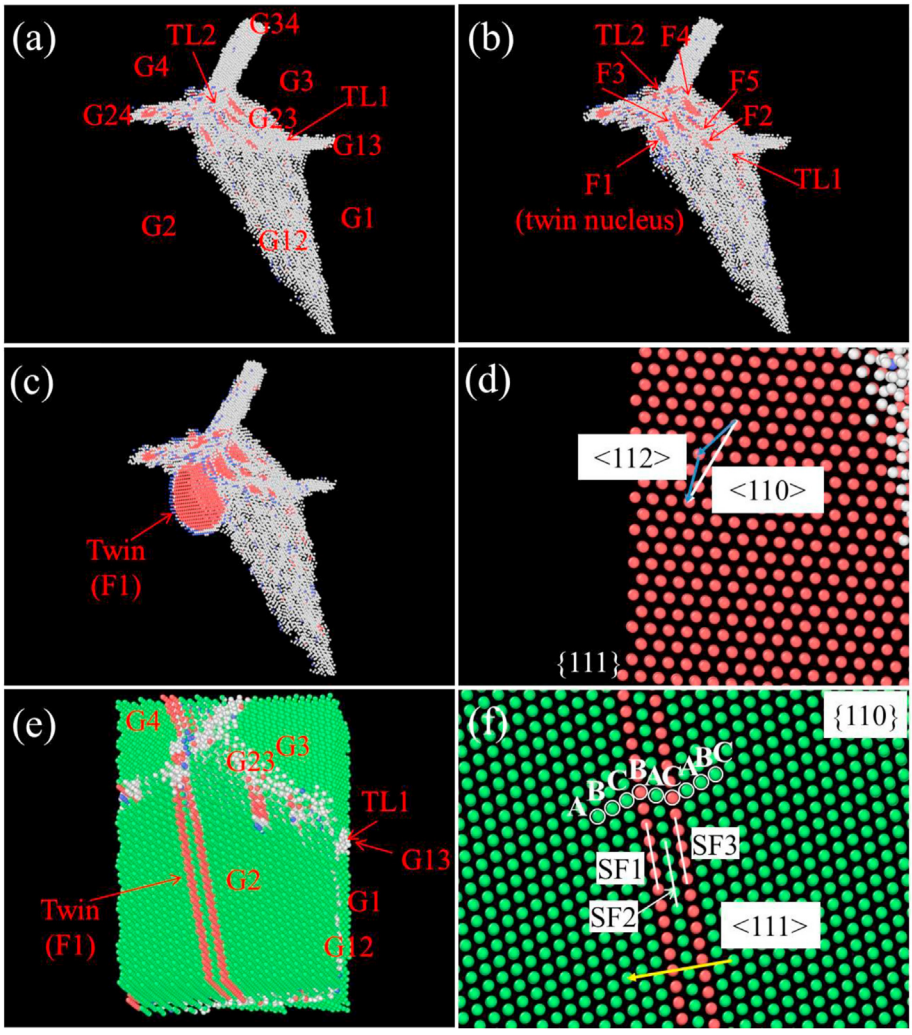

Fig. 1 – The twin nucleated from the triple line TL1. (a) Under 3% shear strain, local areas of red atoms with short range order were observed in the crystal plane of G23. G13, G12, G24, G23 and G34 were GBs between grains G1, G2, G3 and G4. TL1 and TL2 were triple lines abounded by GBs of G13, G12, G23 and GBs of G23, G24, G34, respectively. (b) Under 4% shear strain, red local areas grew and became enlarged to be structure fluctuations. There were 5 structure fluctuations in G23, of which F1 and F2 were emitted from TL1. (c) Under 6% shear strain, the structure fluctuation F1 grew and formed a micro-twin from TL1. (d) The close-packed plane {111} of the twin (F1) in (c), white and blue arrows represent <110> and <112>, respectively. This figure is viewed from the right side of (c). (e) The edge-on view of (c) to show micro-twin with green fcc atoms at grain interior. (f) The zoom-in view of the micro-twin (F1) in (e). The plane is {110}, and the yellow arrow represents <111> which is perpendicular to the twin boundary.

rows of red atoms in Fig. 1(f)) and the initial layer C atoms slipped to an A layer position (i.e. the row of red atoms on the right in Fig. 1(f)). This process thus formed the stacking fault SF1, two partial dislocations and the new stacking sequence ABC‖BCABCA … (‖ stands for the stacking fault location). The slipping process cannot be fully characterized by the view of {110} plane as in Fig. 1(f), while it was more evident from the view of {111} plane as in Fig. 1(d). The second stacking fault SF2 started one layer after the first one ABC‖BCABCA … and changed the stacking sequence to ABC‖B‖ABCAB …. The twin in Fig. 1(f), with the stacking sequence ABC‖B‖A‖CABC …, was formed by the third stacking fault SF3. The short range BCB (ABCBACABC …) and ACA (ABCBACABC …) stacking sequences were where the twin boundaries located. In the MD simulation, they were labeled as red hcp atoms inside grains.

Fig. 1(e) is the edge-on view of the twin in Fig. 1(c). It was composed by three layers (ABCBACABC …, one fcc layer and two hcp boundary layers) of atoms as green fcc atoms were displayed in Fig. 1(e). Individual stacking faults may or may not grow into a twin, depending on the stress condition. In polycrystalline Cu, irrespective of nano or coarse scale, the majority of stacking faults cannot develop into twins. On the basis of atom sites, the partial dislocation is 1/6<112> Shockley partial dislocation. Ref. [1] recorded two dislocation reaction and cross-slip mechanisms to supply or emit continuously twinning partials from the adjacent slip planes at the GBs to grow a twin. Dislocation reactions behind twin growth are out of the scope of discussion.

We inspected nucleation sites of all twins in 6 nc grains of the model by considering the twinning as an evolving process with time and shear strain in three-dimensional space. There were 28 twins in total formed in the simulation and 27 of them were depicted in Fig. 2(a-e). Arabic numbers from 1 to 22 indicated twins nucleating and then being emitted from triple lines, while Roman numerals from I to V implied twins nucleating and being emitted from traditional GBs. The last

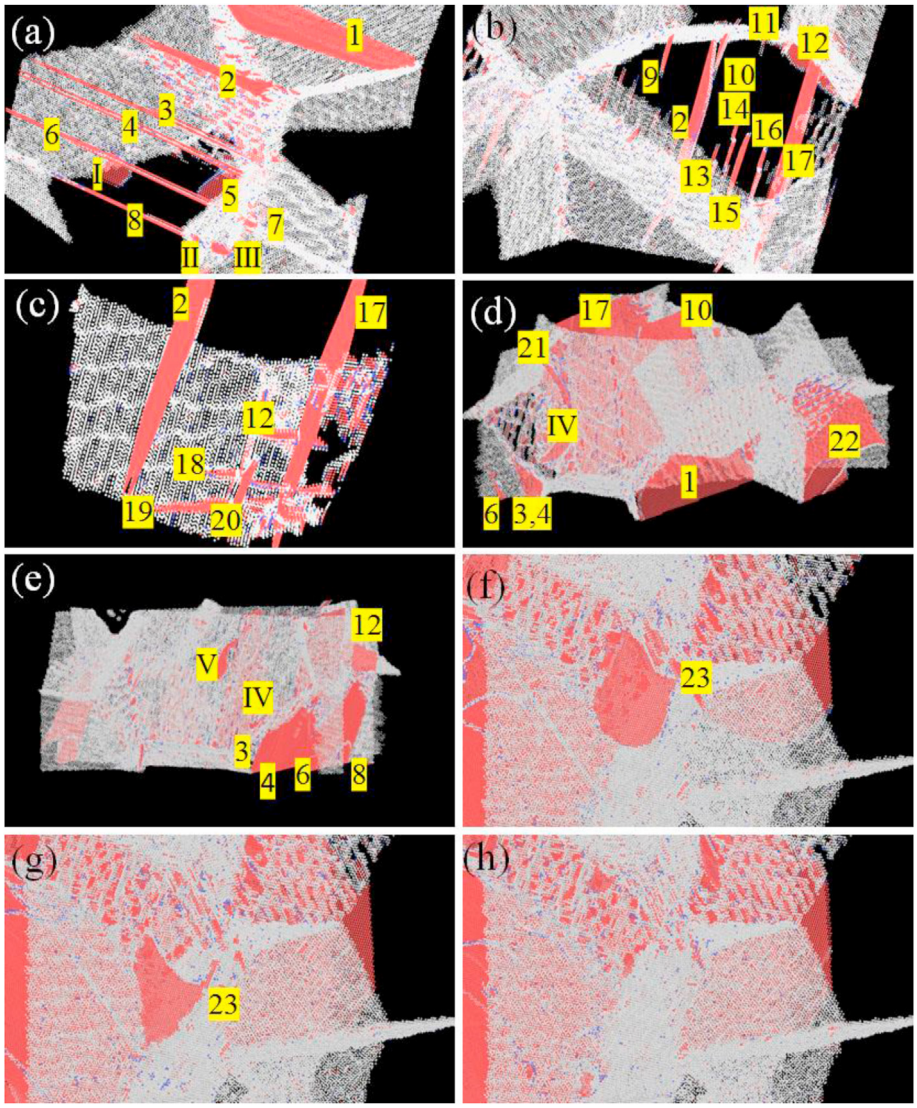

Fig. 2 – (a–f) 28 twins in 6 nc grains of the simulation model. 1–23 represented twinning from triple lines, I–V represented twinning from traditional GBs (f–h) Detwinning process of twin No. 23 under the shear strains of 6.5% (f), 6.8% (g) and 7.4% (h).

one (twin No. 23), as shown in Fig. 2(f-h), was emitted from triple line, but gradually detwinned and consequently disappeared as the strain reached 7.4%. In some cases, two ending twin faults coincided with each other and deceived the twin as the illusion of one layer stacking fault in Fig. 2.

There were two different phenomena when discussing about twins being emitted from GBs. As shown in Fig. 3(a,b), the first phenomenon was about the nucleation of twins No. I-III from GBs. Taken the twin No. I for example, its nucleation site located at the GB gapped between two parts of twin No. 6. That site once was the joint of a GB and the twin No. 6 boundary. Detwinning process left the GB gap along the twin No. 6 boundary. It has been reported that detwinning process could be the result of partial dislocation migration along coherent and incoherent twin boundaries [28] and it just required a relatively small reverse resolved shear stress by comparing to twinning [29]. The other phenomenon could be extracted from twins No. IV and V in Fig. 3(c,d). As demonstrated, new triple lines were formed next to twins No. 10 and 16 in Fig. 3(c,d), respectively. As in the case of twin No. 16, it has already separated its parent matrix into two parts (one part between twins No. 10 and 16, the other part between twins No. 16 and 17), these two parts and the twin No. 16 made the yellow line as a new triple line along the grain next to twin No. 16. Therefore, the twin No. V was emitted from the nucleation site along the new triple line formed by the joint of twin boundary and GB. It has been reported that triple line could be formed by adjoining twin boundary in nc Pd [27]. As classified by Louisette Priester [14] on the basis of the coincidence concept, triple junctions/lines can be sorted into three types: general junction/line between three general boundaries, mixed junction/line between general and coincidence (or near coincidence) site lattice (CSL) boundaries and special junction/line between three special CSL boundaries. In all 28 twins, twins No. 1–23 were emitted from general triple lines, twins No. IV and V were emitted from mixed triple lines, nucleation sites of twins No. I-III were located at traditional GBs [14,31]. Therefore, 25 out of 28 twins were emitted from triple lines after nucleation in our MD simulation.

3.2. *Driving factors*

To investigate the driving factor for above phenomena, the method of Herring's equilibrium rule was adopted to explore the variations of dihedral angles and relative GB energy around a triple line before and after twinning [13,14]. Fig. 4 captures the triple line which is the connection of GBs belonging to grains G1, G2 and G3. It emitted twins No. 10 and 13–16. Before twinning, dihedral angles around the triple junction/line were θ_{13} (145°), θ_{12} (137°) and θ_{23} (78°), the GB energy per area were γ_{13}, γ_{12} and γ_{23}. According to Herring's equilibrium rule, the balance of interfacial energy at an equilibrated triple junction/line was thus given by:

$$\frac{\gamma_{13}}{\sin\theta_{13}}=\frac{\gamma_{12}}{\sin\theta_{12}}=\frac{\gamma_{23}}{\sin\theta_{23}} \quad (1)$$

After twins being emitted, corresponding dihedral angles were θ'_{13} (140°), θ_{1T} (135°) and θ_{3T} (85°), the grain and/or twin boundary energy per area were γ_{13}, γ_{1T} and γ_{3T}. Assuming that the local thermal equilibrium would be fulfilled at the triple line regardless of twinning, Herring's equilibrium rule could

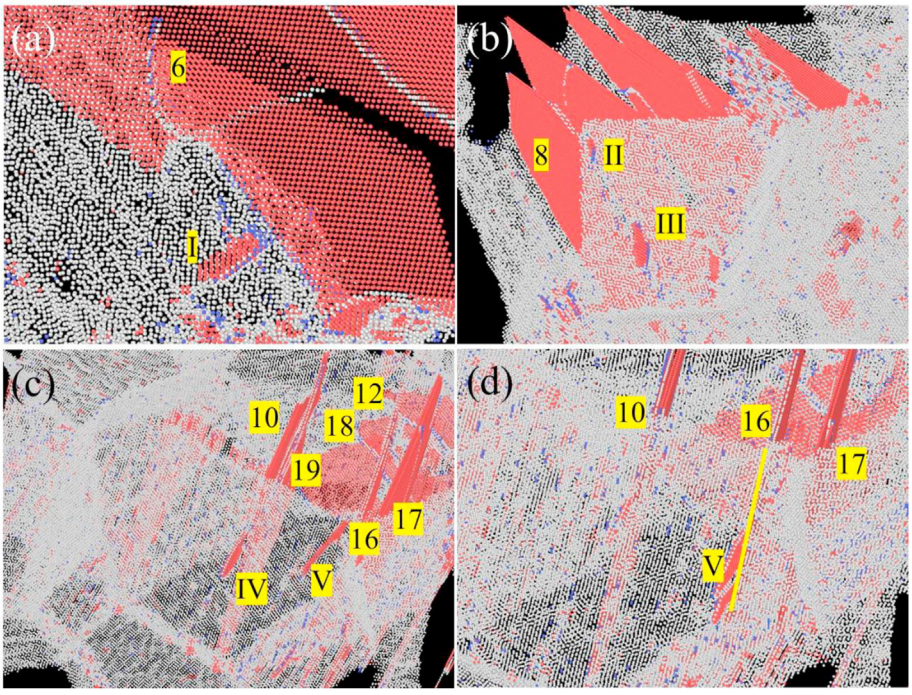

Fig. 3 – (a) Twin No. I was emitted from the GB which has been the gap between two parts of twin No. 6 after detwinning; (b) twins No. II and III were emitted from GB; (c) twins No. IV and V were emitted from new triple lines; (d) twin No. V was emitted from the new triple line (denoted by the yellow line) formed by twin No. 16.

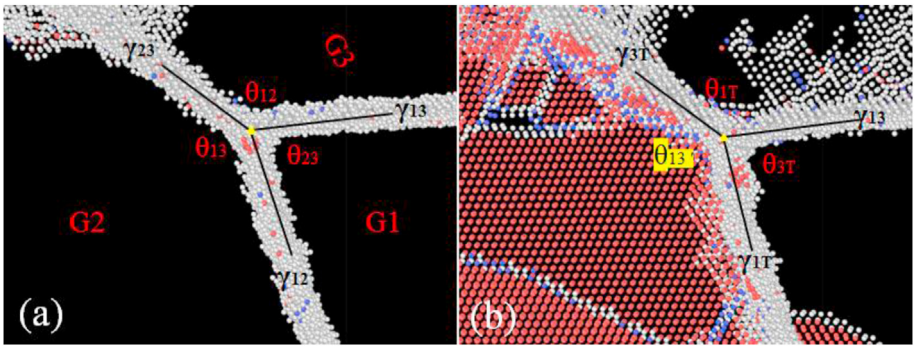

Fig. 4 – Illustrations of dihedral angles and relative GB energy around the triple junction/line which emitted twins No. 10 and 13–16. (a) Before twinning, the dihedral angles θ_{13}, θ_{12}, θ_{23} and their relative GB energy per area γ_{13}, γ_{12}, γ_{23}. (b) After twinning, the dihedral angles θ_{13}', θ_{1T}, θ_{3T} and their relative GB energy per area γ_{13}, γ_{1T}, γ_{3T}.

be applied to describe the relationship between energy and geometry of the interface before/after twinning [13,14]. As stated in [13,30], a decrease in the total energy should lead to observable changes in dihedral angles such that $\theta'_{13} < \theta_{13}$ and $\theta_{12} + \theta_{23} < \theta_{1T} + \theta_{3T}$, this observation agreed well with results herein. It has been noted that there was no necessary for each single boundary to reduce its energy, however, the energy sum ($\gamma_{1T} + \gamma_{3T}$) after twinning should be less than its counterpart ($\gamma_{12} + \gamma_{23}$) [13]. From Eq. (1), the energy sum could be deduced:

$$\gamma_{12} + \gamma_{23} = \gamma_{13} \times \frac{\sin\theta_{12} + \sin\theta_{23}}{\sin\theta_{13}} \tag{2}$$

Because γ_{13} stayed the same before and after twinning, the quantity ($\sin\theta_{12} + \sin\theta_{23}$)/$\sin\theta_{13}$ and ($\sin\theta_{1T} + \sin\theta_{3T}$)/$\sin\theta'_{13}$ could be used to compare the relative GB energy sum before and after twinning. The former one was 2.89 and the latter one was 2.65. This implied that twinning from triple line had reduced the relative GB energy. It was consistent with earlier work [13]. Partial dislocation emission, forming either stacking faults or twins in neighboring grains, was proposed to trigger GB relaxation via GB dissociation processes to lower energy states [13,33].

As each single twin in coarse grain could induce more concentrated stress, it would be easier to recognize changes of dihedral angles and relative GB energy sum in coarse grains. To better understand this change in nc grains, this work analyzed on the triple line which has nucleated and emitted multiple twins No. 10 and 13–16. In fact, Eq. (1) highly depends on thermal equilibrium condition and neglects the existence of a torque term [14]. It was imperfect to be applied to the junctions/lines between the coherent and incoherent twins, which were frequently presented in fcc metals [14]. Therefore, cases of twinning from mixed triple lines (twins No. IV and V) called for a more general explanation.

As grain cell remained nearly unchanged during twinning, local stress and energy should be affected by typical microstructural entity (GB, triple line and newly formed twin). The more general explanation for driving force of above phenomena could be obtained by calculating the change of average atomic stress and potential energy of the referred microstructural entity during twinning. Atomic stress and potential energy could be calculated by the position and velocity of each atom obtained from MD simulation. The von Mises stress representing the shear stress on each atom could be simplified as [12]:

$$\sigma_{vm}(i) = \left\{\frac{1}{2}\left[(\sigma_{xx}(i) - \sigma_{yy}(i))^2 + (\sigma_{yy}(i) - \sigma_{zz}(i))^2 + (\sigma_{xx}(i) - \sigma_{zz}(i))^2 + 6\left(\sigma_{xy}^2(i) + \sigma_{zy}^2(i) + \sigma_{zx}^2(i)\right)\right]\right\}^{1/2} \tag{3}$$

Fig. 5 illustrates the average atomic von Mises stress and the average atomic energy imposed on each atom of the

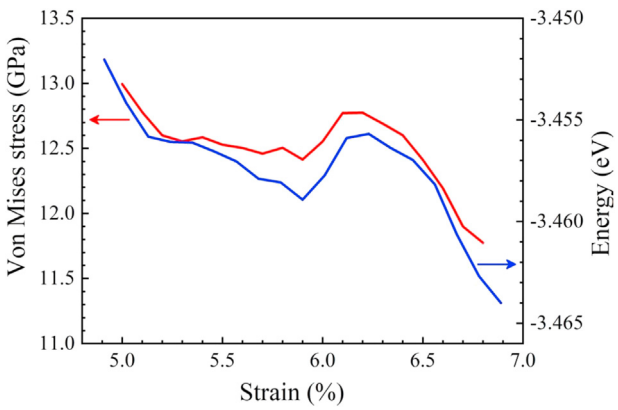

Fig. 5 – Evolutions of average atomic von Mises stress (red line) and average atomic energy (blue line) with the shear strain.

microstructural entity above. As discussed, the microstructural entity was composed by three GBs and the triple line before twinning, while twins No. 10 and 13–16 would gradually be included in the microstructural entity with the evolution of strain and twinning. The average atomic von Mises stress and the average atomic energy were 12.99 GPa and −3.452 eV at the strain of 5.0% before twinning. They decreased to 12.41 GPa and −3.459 eV by twinning (Fig. 6(a)) at the strain of 6.0%. Then twin No. 16 began to detwin (Fig. 6(b)), which caused raises of the average atomic von Mises stress and the average atomic energy to 12.77 GPa and −3.455 eV at the shear strain of 6.1%. Finally, many twin embryos turned into nuclei and it promoted twins being emitted from the triple line, as shown in Fig. 6(c) under the shear strain of 6.6%. Multiple twinning drastically reduced the average atomic von Mises stress and the average atomic energy when the strain surpassed 6.2%.

3.3. *TKD characterization*

Fig. 7(a) illustrates the orientation mapping of Cu after HPT, inset is the IPF-Z (inverse pole figure) color code legend which relates the orientation and color. In the IPF-Z color code legend, red, green and blue indicate grains having <001>, <101> and <111> directions parallel to the axis Z (being perpendicular to the orientation map). The black, silver and red lines in Fig. 7(a) represent the high angle GBs (>10°), low angle GBs (from 2° to 10°) and twin boundaries, respectively.

Letters A-C highlight three typical twin morphologies which highly depended on the twin thickness and TKD step size. In fact, to be characterized by the TKD, the twin should be detected having misorientation across its boundary against the grain matrix. If its thickness were smaller than the TKD step size, it would be missed due to the limitation of resolution. When the twin thickness was around or slightly larger than the TKD step size, the twin domain could be resolved as pixels by the TKD. The twin would entirely be represented by a single red $\sum 3$ line bounded by two separate matrices with identical orientation as in the case A. Secondly, when the twin thickness was much larger than the TKD step size, it could be characterized as a twin domain with two bounding red $\sum 3$ lines (case B). Lastly, the case C occurred when the twin propagated to the GB and grew to cover part of the grain. In this case, only a single red $\sum 3$ line split the grain, half being the grain matrix and the other half being the twin domain. The twin morphology is consistent with our earlier work [18] which was supported by the evidence from high resolution transmission electron microscope. Fig. 7(b) is the histogram of grain size distribution in Fig. 7(a). Since the step size was 6 nm, we excluded the data of grain size smaller than 30 nm.

On the basis of statistical data, the HPTed Cu was mainly composed of nc grains. According to our MD results, the twins should tend to intersect with the triple lines of the nc grains. Triple lines could hardly be captured or could be merely characterized as the existence of triple junctions in the EBSD orientation map, as it was just two-dimensional map. We inspected nc grains and twins from TKD data, 197 twins were identified in nc grains. As discussed, TKD in this research was unable to characterize stacking faults and micro-twins whose sizes were less than the 6 nm step size (about 20 layers of

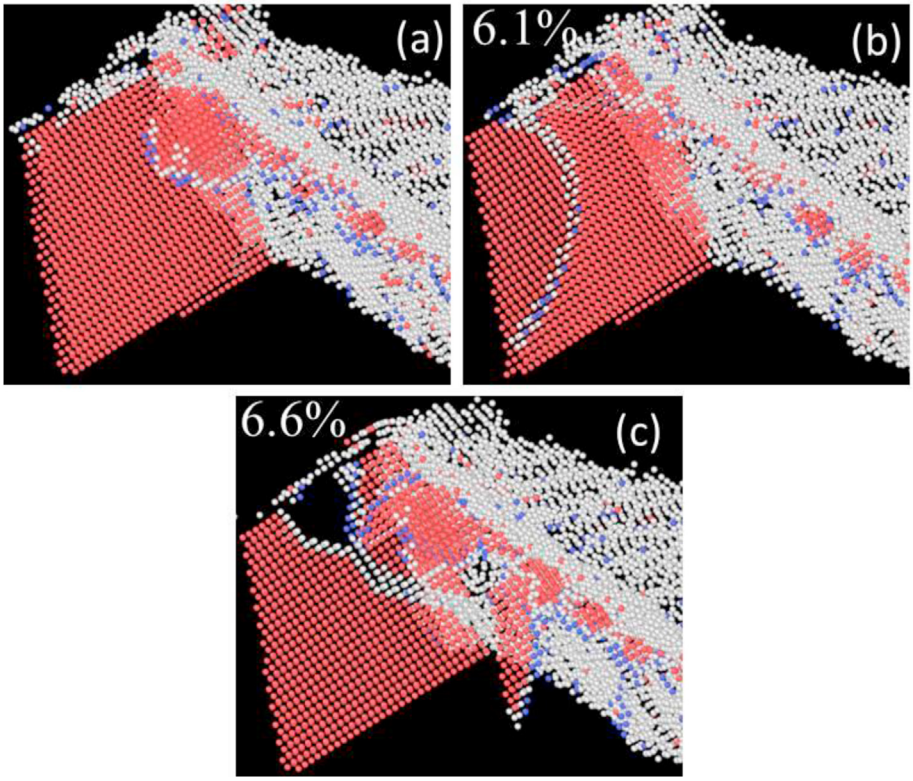

Fig. 6 – Evolutions of typical microstructural entity corresponding to strains of (a) 6.0% (twin No. 16 began to detwin), (b) 6.1% (detwinning process of twin No. 16) and (c) 6.6% (formation of twins No. 10 and 13–15).

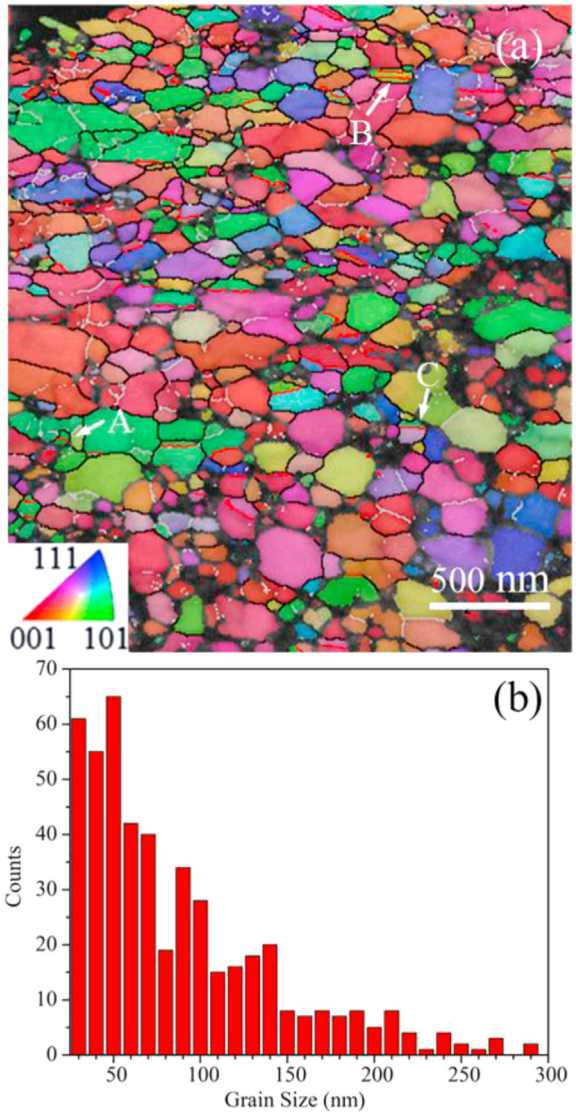

Fig. 7 – (a) The orientation mapping of Cu after HPT, inset is the IPF-Z color code legend. The black, silver and red lines represent the high angle GBs (>10°), low angle GBs (from 2° to 10°) and twin boundaries, respectively. Letters A-C highlight three typical twin morphologies. (b) The grain size distribution of (a).

atoms). Therefore, the characterized twin density was less dense than the real condition. Though the absolute values of twins and triple junction-twin intersections were reduced, the relative value or fraction of triple junction-twin intersections was hardly affected.

The statistical date of the triple junction-twin intersection is listed in Table 1. The fraction of the triple junction-twin intersection was 81.7%, being lower than our MD prediction. The underestimation should be caused by the invisible triple lines in the orientation mapping. No matter MD simulation but also TKD characterization demonstrated the preferred twining from triple lines. On the basis of thermodynamics, twinning from both triple lines and GBs would help the system reduce energy and stay in an equilibrium position. As stated, however, triple lines are energetically more favorable than GBs. From the perspective of kinetics, it would be easier, faster, more frequent and probable to emit twins from triple lines. The higher probability could be caused by either more structure fluctuations, twin embryos and nuclei or higher energy reduction.

Table 1 – Statistical data of triple junctions intersected with twins. Y and N in this table denote whether a twin (boundary or domain) was connected to a triple junction.

Twinned nanograins (Counts)	Y		N	
	Counts	Fraction (%)	Counts	Fraction (%)
197	161	~81.7	36	~18.3

4. Conclusion

To conclude, from MD simulation of nc Cu, we found that twins No. I-III were emitted from traditional GBs (non-CSL boundaries), while twins No. IV, V and 1–23 were emitted from mixed triple lines between traditional and CSL/near CSL boundaries, and from general triple lines between three traditional boundaries, respectively. The atomic map of microstructure evolution on twinning process has been discussed. Before twinning, the stress concentration and extra energy made triple lines the preferred nucleation sites for twin embryos. During twinning, the stress relaxation and energy reduction provided the driving force for twins being emitted from triple lines. Twinning from general triple lines could be supported by the reduction of dihedral angle (θ_{13} - θ'_{13}) and relative GB energy sum [($\sin\theta_{12} + \sin\theta_{23}$)/$\sin\theta_{13}$ - ($\sin\theta_{1T} + \sin\theta_{3T}$)/$\sin\theta'_{13}$]. Furthermore, more general explanation for twins being emitted from either general or mixed triple lines could be ascribed to the average atomic von Mises stress and the average atomic energy of typical microstructural entity, which had the tendency to decrease during twinning. The twinning from triple lines was further verified by the TKD characterization of nc Cu after HPT. It underestimated the phenomenon because triple lines parallel to the vision were invisible.

Declaration of Competing Interest

The authors declare that they have no known competing financial interests or personal relationships that could have appeared to influence the work reported in this paper.

Acknowledgements

Y.H. Zhao acknowledges financial supports from the National Key R&D Program of China (Grant No. 2017YFA0204403) and the National Natural Science Foundation of China (Grant No. 51971112 and 51225102) as well as the Fundamental Research

for the Central Universities (No. 30919011405). Authors declare no conflict of interests.

REFERENCES

[1] Zhu YT, Liao XZ, Wu XL. Deformation twinning in nanocrystalline materials. Prog Mater Sci 2012;57:1–62.
[2] Yamakov V, Wolf D, Phillpot SR, Mukherjee AK, Gleiter H. Dislocation processes in the deformation of nanocrystalline aluminium by molecular-dynamics simulation. Nat Mater 2002;1:45–9.
[3] Swygenhoven HV, Derlet PM, Hasnaoui A. Atomic mechanism for dislocation emission from nanosized grain boundaries. Phys Rev B 2002;66. 024101.1–024101.8.
[4] Liao XZ, Zhou F, Lavernia EJ, Srinivasan SG, Baskes MI, He DW, et al. Deformation mechanism in nanocrystalline Al: partial dislocation slip. Appl Phys Lett 2003;83:632–4.
[5] Liao XZ, Zhou F, Lavernia EJ, He DW, Zhu YT. Deformation twins in nanocrystalline Al. Appl Phys Lett 2003;83:5062–4.
[6] Wu XL, Zhu YT. Partial-dislocation-mediated processes in nanocrystalline Ni with nonequilibrium grain boundaries. Appl Phys Lett 2006;89. 31922.1–31922.3.
[7] Huang JY, Zhu YT, Jiang H, Lowe TC. Microstructures and dislocation configurations in nanostructured Cu processed by repetitive corrugation and straightening. Acta Mater 2001;49:1497–505.
[8] Gutkin MY, Ovid'ko IA, Skiba NV. Emission of partial dislocations by grain boundaries in nanocrystalline metals. Phys Solid State 2004;46:2042–52.
[9] Ovid'ko IA, Sheinerman A. Suppression of nanocrack generation in nanocrystalline materials under superplastic deformation. Acta Mater 2005;53:1347–59.
[10] Gottstein G, Shvindlerman LS, Zhao B. Thermodynamics and kinetics of grain boundary triple junctions in metals: recent developments. Scripta Mater 2010;62:914–7.
[11] Palumbo G, Aust KT. Triple-line corrosion in high purity nickel. Mater Sci Eng, A 1989;113:139–47.
[12] Guo YB, Xu T, Li M. Generalized type III internal stress from interfaces, triple junctions and other microstructural components in nanocrystalline materials. Acta Mater 2013;61:4974–83.
[13] Lin B, Jin Y, Hefferan CM, Li SF, Lind J, Suter RM, et al. Observation of annealing twin nucleation at triple lines in nickel during grain growth. Acta Mater 2015;99:63–8.
[14] Priester L. The triple junction. In: Grain boundaries. Dordrecht: Springer Netherlands; 2013. p. 305–36.
[15] Gutkin MY, Ovid'ko IA, Skiba NV. Crossover from grain boundary sliding to rotational deformation in nanocrystalline materials. Acta Mater 2003;51:4059–71.
[16] Kumar KS, Suresh S, Chisholm MF, Horton JA, Wang P. Deformation of electrodeposited nanocrystalline nickel. Acta Mater 2003;51:387–405.
[17] Wang L, Zhou J, Zhang S, Liu Y, Dong S. Effects of accommodated grain boundary sliding on triple junction nanovoid nucleation in nanocrystalline materials. Mech Mater 2014;71:10–20.
[18] Liu SL, Ma XL, Li LZ, Zhang LW, Trimby PW, Liao XZ, et al. Effect of triple junctions on deformation twinning in a nanostructured Cu–Zn alloy: a statistical study using transmission Kikuchi diffraction. Beilstein J Nanotechnol 2016;7:1501–6.
[19] Greer AL. Triple lines in nucleation. Scripta Mater 2010;62:899–903.
[20] Plimpton S. Fast parallel algorithms for short-range molecular dynamics. J Comput Phys 1995;117:1–19.
[21] Zhou XW, Wadley HNG, Johnson RA, Larson DJ, Tabat N, Cerezo A, et al. Atomic scale structure of sputtered metal multilayers. Acta Mater 2001;49:4005–15.
[22] Stukowski A. Visualization and analysis of atomistic simulation data with OVITO–the open visualization tool. Model Simulat Mater Sci Eng 2010;18. 15012.1–15012.7.
[23] Faken D, Jónsson H. Systematic analysis of local atomic structure combined with 3D computer graphics. Comput Mater Sci 1994;2:279–86.
[24] Tsuzuki H, Branicio PS, Rino JP. Structural characterization of deformed crystals by analysis of common atomic neighborhood. Comput Phys Commun 2007;177:518–23.
[25] Atomsk Hirel P. A tool for manipulating and converting atomic data files. Comput Phys Commun 2015;197:212–9.
[26] Miura H, Sakai T, Jonas J. Variant selection of dynamically nucleated twins at triple junctions in a copper tricrystal. Scripta Mater 2006;55:167–70.
[27] Wang Y, Su Z, Ping D. Microstructure investigation on the triple junction with an adjoining twin boundary in nanocrystalline Palladium. J Mater Sci Technol 2010;26:1047–50.
[28] Yoo BG, Boles ST, Liu Y, Zhang X, Schwaiger R, Eberl C, et al. Quantitative damage and detwinning analysis of nanotwinned copper foil under cyclic loading. Acta Mater 2014;81:184–93.
[29] Wang L, Lind J, Phukan H, Kenesei P, Park JS, Suter RM, et al. Mechanical twinning and detwinning in pure Ti during loading and unloading – an in situ high-energy X-ray diffraction microscopy study. Scripta Mater 2014;92:35–8.
[30] Murr LE. Energetics of grain boundary triple junctions and corner twinned junctions: transmission electron microscope studies. J Appl Phys 1968;39:5557–66.
[31] Li XY, Wei YJ, Lu L, Lu K, Gao HJ. Dislocation nucleation governed softening and maximum strength in nano-twinned metals. Nat 2010;464:877–80.
[32] Wlide G. Physical metallurgy of nanocrystalline metals. In: Physical metallurgy. Elsevier; 2015. p. 2707–804.
[33] Zhou X, Li XY, Lu K. Size dependence of grain boundary migration in metals under mechanical loading. Phys Rev Lett 2019;122. 126101.1–126101.6.